Local structure and magnetism of Co^{3+} in wurtzite Co:ZnO

Bastian Henne,[1,*] Verena Ney,[1] Julia Lumetzberger,[1] Katharina Ollefs,[2,†] Fabrice Wilhelm,[2] Andrei Rogalev,[2] and Andreas Ney[1]

[1]*Institut für Halbleiter- und Festkörperphysik, Johannes Kepler Universität, Altenberger Strasse 69, 4040 Linz, Austria*

[2]*ESRF – The European Synchrotron CS40220, 38043 Grenoble Cedex 9, France*

(Received 18 August 2016; revised manuscript received 14 December 2016; published 3 February 2017)

The structural and magnetic properties of 30% and 50% Co-doped ZnO have been investigated in order to determine the influence of the presence of Co^{3+} as a potential *p*-type dopant. For 30% doping, Co^{3+} could be stabilized in the wurtzite lattice of ZnO without phase separation by providing high oxygen partial pressures during growth. At 50% Co concentration, the crystal lattice destabilizes. X-ray absorption spectroscopy and simulations are used to substantiate the valence and local structure of Co^{3+}. Integral and element selective magnetometry reveals uncompensated antiferromagnetism of the Co atoms irrespective of being present as Co^{2+} or Co^{3+}.

DOI: 10.1103/PhysRevB.95.054406

I. INTRODUCTION

Over the past few decades there have been primarily two goals stimulating intensive research efforts in doped ZnO semiconductors: the ability to achieve *p*-type conductivity [1] and the ability to obtain magnetic order [2,3], preferably at room temperature. Many avenues have been followed to accomplish these objectives, and several mechanisms, such as defects [4] or carrier mediation [5], have been proposed to explain the occasional observations of long-range magnetic order, often based on large hole concentrations [6] or oxygen vacancies in doped ZnO [7]. For $ZnCo_2O_4$, on the other hand, which is widely known as anode material in lithium batteries [8] and as crystalline, or amorphous *p*-type gate in junction field-effect transistors [9], it has also been reported that the provided oxygen partial pressure during growth can change the conduction type and even the magnetic properties from paramagnetic to ferromagnetic [10]. Other studies, however, observed weak antiferromagnetism at low temperatures when no extra oxygen is provided [11,12]. For Co-doped ZnO (Co:ZnO), the opposite magnetism/oxygen pressure dependence was found: with increasing oxygen pressure, the ferromagnetic signatures observable at low pressures vanished, which led to the conclusion that oxygen vacancies are necessary to induce ferromagnetic coupling [13].

Recently, a strong correlation between the local coordination of Co atoms and the carrier type in the Zn-Co-O system was established [12]. Throughout the compositional range from 60% Co:ZnO to $ZnCo_2O_4$, it could be shown that samples in which the Co atoms are tetrahedrally coordinated via oxygen atoms, as in regular wurtzite ZnO, are in the Co^{2+} valence state and the samples proved to be *n*-type, whereas samples with predominantly octahedral Co coordination, such as Co^{3+} in the $ZnCo_2O_4$ spinel, show *p*-type conductivity. A drawback in Ref. [12] was the extremely high Co concentration in ZnO, leading to a tendency to form the $ZnCo_2O_4$ spinel and mixed crystalline phases.

All those studies suggest that reliable control of the magnetic cations' local coordination seems to be a vital ingredient and a promising avenue to fine-tune the electrical and magnetic properties in transition-metal doped oxides. The realization of stable Co^{3+} in a wurtzite environment is therefore a promising concept to tackle the ongoing issue of *p*-type doping ZnO and to study the potential for hole-mediated magnetic order in doped ZnO.

Here we present a study on the structural and magnetic properties of Co:ZnO with a focus on the reliable control of the local coordination of the dopant atom and the resulting majority carrier type. For 30% Co concentration, i.e., below the $ZnCo_2O_4$ cationic stoichiometry, the formation of the spinel phase is not observed, while for 50% Co concentration the wurtzite structure destabilizes upon the formation of Co^{3+}. X-ray absorption spectroscopy and simulations are used to substantiate the desired stabilization of Co^{3+} in the wurtzite structure of ZnO. The Seebeck coefficient indicates that the majority charge carrier in these specimens is *p*-type. SQUID magnetometry and element-selective x-ray magnetic circular dichroism (XMCD) are used to characterize the resulting magnetic properties, which are found to be that of an uncompensated antiferromagnet irrespective of Co being in its Co^{2+} or Co^{3+} configuration.

II. EXPERIMENTAL DETAILS

Two series of epitaxial films of $Zn_{1-x}Co_xO$, $x \in 0.3,0.5$ (30/50% Co:ZnO) with a nominal thickness of 200 nm have been grown by reactive magnetron sputtering on polished *c*-sapphire (001) substrates in an ultrahigh-vacuum system ($p_{base} \sim 2\times10^{-9}$ mbar) using metallic composite targets (Zn:Co = 70:30/50:50). To alter the Co valence, the Ar:O_2 ratio was systematically varied by individual mass-flow controllers from 10:1 to 10:6 (30%) and from 10:0.8 to 10:4 (50%) standard cubic centimeters per minute (sccm) while

*bastian.henne@jku.at

†Present address: Faculty of Physics and Center for Nanointegration Duisburg-Essen (CENIDE), Universität Duisburg-Essen, Lotharstrasse 1, 47048 Duisburg, Germany.

Published by the American Physical Society under the terms of the Creative Commons Attribution 3.0 License. Further distribution of this work must maintain attribution to the author(s) and the published article's title, journal citation, and DOI.

the process pressure was kept constant at 4×10^{-3} mbar. The growth temperature was held constant at 450 °C (30%) and 294 °C (50%) for all samples; this was optimized to yield the best crystalline quality throughout the growth series.

The crystalline quality was investigated by x-ray diffraction (XRD) using a PANalytical X'Pert Pro MRD to record $\omega/2\theta$ and ω-rocking scans. X-ray absorption near-edge spectroscopy (XANES) measurements were conducted at beamline ID12 at the European Synchrotron Radiation Facility (ESRF) in Grenoble under 15° grazing incidence using total fluorescence yield detection [14]. The x-ray linear dichroism (XLD) was derived by taking the direct difference of two normalized XANES recorded with two orthogonal linear polarizations at 300 K. A quarter wave plate was used to flip the linear polarization of the synchrotron light from vertical to horizontal, i.e., from parallel to perpendicular to the surface normal of the film. The XMCD was taken as the direct difference of XANES recorded with right and left circular polarized light at 2 K and 17 T. To minimize the artifacts, the direction of the external magnetic field was reversed as well. Element-selective magnetization curves at 2 K were recorded by flipping the circular polarization at fixed photon energies in magnetic fields of up to 17 T. Integral magnetization measurements from 300 to 2 K were performed using a commercial SQUID magnetometer (Quantum Design, MPMS-XL5) applying up to 5 T in the film plane to record magnetization curves. The $M(T)$ dependence is measured at 10 mT while warming the sample from 2 to 300 K after cooling down in 5 T (FH) and 0 mT (ZFC). Subsequently, $M(T)$ is measured from 300 to 2 K at 10 mT (FC). The diamagnetic background of the substrate, derived from high-field $M(H)$ data at 300 K, has been subtracted from all magnetization data [15]. Finally, to determine the majority carrier type of the samples, the sign of the Seebeck coefficient has been determined using an ordinary hot tip (360 °C)/cold tip (RT) setup on Ohmic gold contacts in a 5 mm × 5 mm van der Pauw geometry.

III. RESULTS AND DISCUSSION

Figure 1 displays the x-ray diffractograms of the 30% Co:ZnO growth series from Ar:O_2 = 10:1 to 10:6. It is evident that only the reflections belonging to *c*-ZnO and the sapphire substrate are observed, indicating the absence of other crystalline phases, such as cubic CoO, on a global scale. In particular, a change in crystal structure, i.e., the occurrence of a $ZnCo_2O_4$ spinel phase as observed for 60% Co concentrations around 38° [12], is not present for the 30% Co series. The full width at half-maximum (FWHM) of the main reflection at ∼34° serves as a measure for the crystalline quality of the samples. It increases with increasing Ar:O_2 ratio from 0.18° (10:1) to 0.46° (10:6). The (002) peak position of the 10:1 sample still coincides with the literature value of 34.42° for undoped ZnO [16,17], whereas for all samples grown at higher oxygen partial pressures the peaks shift to lower angles, i.e., a larger *c*-lattice parameter, which we tentatively ascribe to the presence of oxygen interstitials at high oxygen partial pressures.

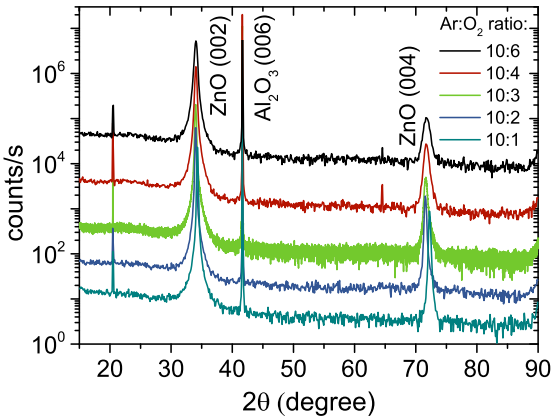

FIG. 1. X-ray diffractograms of 30% Co:ZnO in dependence of the Ar:O_2 ratio.

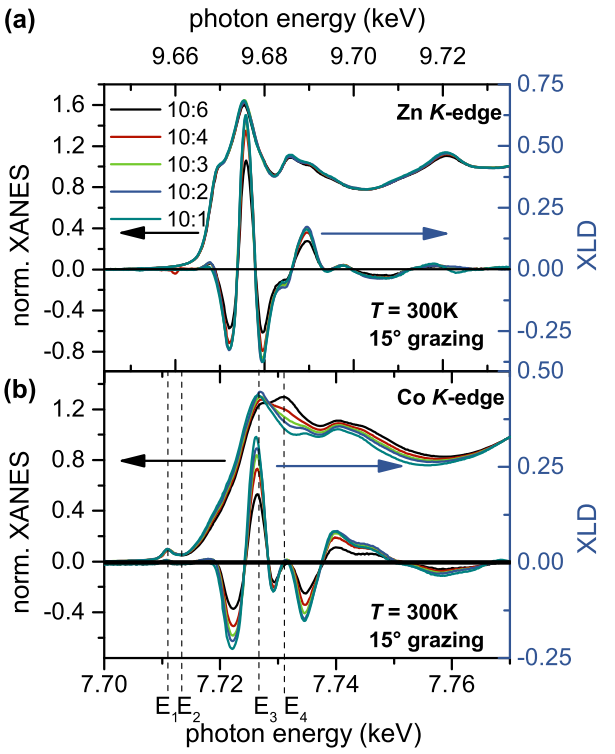

FIG. 2. XANES and XLD measurements performed at the Zn (a) and Co (b) *K*-edge of 30% Co:ZnO with varying Ar:O_2 ratios.

In Fig. 2, XANES and respective XLD measurements at the Zn (a) and Co (b) *K*-edges are shown. The size of the XLD serves as a measure for the crystallinity on a local scale, which reflects the local anisotropy of the crystal field. Similarly to the FWHM in XRD measurements, it decreases for increasing Ar:O_2 ratios from 0.95 (10:1) to 0.68 (10:6) at the Zn edge. For ideal wurtzite ZnO with 10% Co content, a maximum Zn *K*-edge XLD amplitude of 1.11 has been reported [18]. For the Co *K*-edge [Fig. 2(b)], the XLD amplitudes decrease from 0.55 (10:1) to 0.30 (10:6), whereas for samples with low Co concentration it can exceed 0.6 [19]. The reduction of the XLD amplitude at both *K*-edges with increasing Ar:O_2 ratios fits the observation of an increasing FWHM in the XRD measurements. The incorporation of oxygen on interstitial sites may cause a lattice distortion/ stretching and therefore a

concomitant reduction of local crystalline quality as measured by XLD. The presence of a pronounced preedge feature in the Co K-edge XANES (E_1/E_2 in Fig. 2), however, demonstrates via comparison with Ref. [19] that all specimens are devoid of metallic Co precipitations.

Interestingly, the absorption edge in the Co XANES [Fig. 2(b)] shifts gradually to higher energies with increasing oxygen partial pressure, which indicates a continuous valence shift from Co^{2+} towards Co^{3+}. Furthermore, the fine-structure of the XANES changes and a second peak appears at higher energies (E_4). The shift between the two end points, 10:1 and 10:6, can be seen more clearly in Fig. 7(a). While for 60% Co:ZnO the valence shift and the accompanying total disappearance of the XLD could easily be attributed to the formation of the cubic $ZnCo_2O_4$ spinel by XRD [12], here the situation is very different. A finite (wurtzite-like) XLD remains and no spinel signature is detectable by XRD on a global scale (see Fig. 1). To understand the occurring valence shift, simulations of the Co absorption edge have been performed using *ab initio* calculations via the FDMNES code [20]. To perform the simulations with this code, an input file with atomic positions of a supercell with a total of 66 atoms is prepared. After the initial multiple scattering approach on a muffin-tin potential, a convolution is performed to account for the core-hole broadening and the spectral width of the final states [20]. A detailed report on the application of the FDMNES code to Co:ZnO can be found in [21]. First, one additional oxygen atom has been placed on the adjacent tetrahedral interstitial site in the wurtzite structure of Co-doped ZnO [labeled 1^{st} in Fig. 3(a)]. As a next step, a second oxygen atom has been placed on an additional adjacent interstitial site [2^{nd} in Fig. 3(a)], at the center position of the adjoining oxygen tetrahedron, to match a quasioctahedral coordination by introducing six Co-O bonds around one Co dopant. Both resulting spectra significantly deviate from the simulated spectrum of Co:ZnO (green line) but are rather similar (not shown). In Figs. 3(b) and 3(c), the simulated spectra and experimental reference spectra are confronted to compare the specific spectral features. The simulated XANES [blue line in Fig. 3(b)] matches the experimental one of Co^{3+} in $ZnCo_2O_4$ [blue line in Fig. 3(c)] rather well, although no relaxation of the input structure is performed. This simulated spectrum is then superimposed with the simulated spectrum of Co-doped ZnO (green line) in the same way as was reported in Ref. [22]. The superimposed spectrum is plotted as a thick red line in Fig. 3(b). A weighing factor of 34.5% quasioctahedral to 65.5% substitutional Co:ZnO best resembles the experimental spectrum of the specimen with the highest Co^{3+} content [black line in Fig. 3(c)]. All features that occur in the experimental XANES are present in the simulated data with only slight deviations, which might be due to the mentioned nonrelaxed lattice in the simulations. Although no spinel phase forms on a global scale and the wurtzite structure of ZnO is maintained, the correlation between valence and local structure, as established for 60% Co:ZnO in Ref. [12], extends to low Co concentrations. This fortifies the idea that for Co:ZnO a certain amount of Co atoms, as in $ZnCo_2O_4$, is at least bound in a quasioctahedral manner to more than four oxygen atoms when high oxygen partial pressure is provided during growth.

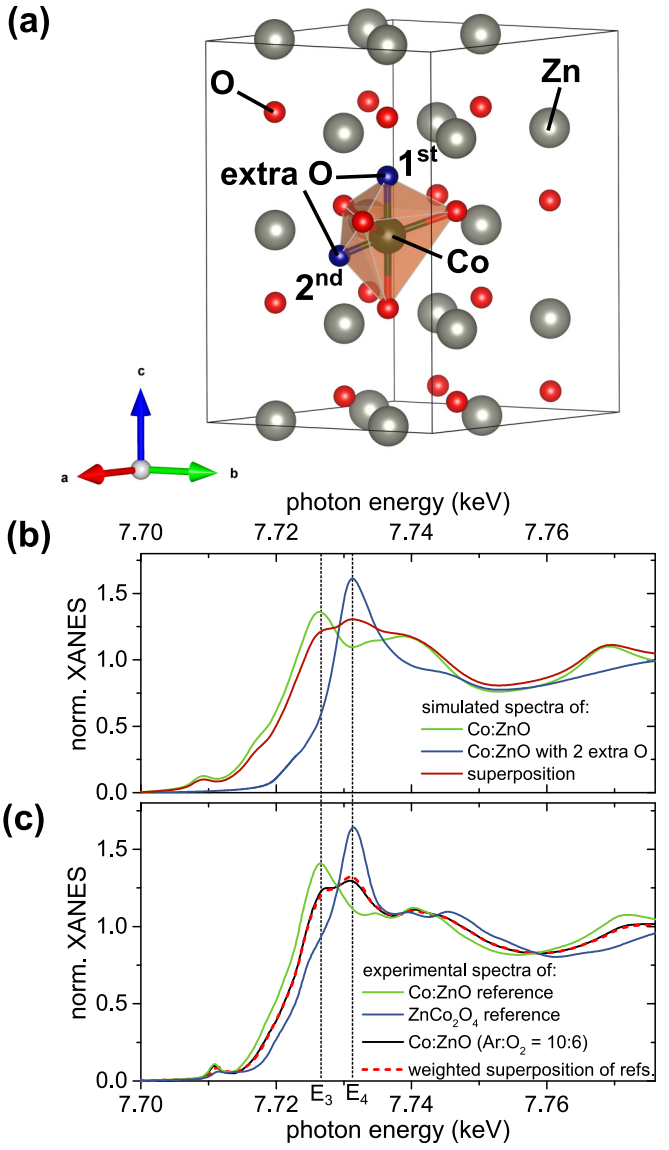

FIG. 3. (a) Position of the two extra oxygen atoms, "1^{st}" and "2^{nd}", in the wurtzite structure of Co:ZnO. The extra atoms are indicated in blue (structure created with VESTA [23]). Comparison between the simulated (b) and the experimental (c) absorption spectrum for Co:ZnO with interstitial oxygen. The dotted vertical lines indicate the positions of the two main absorption peaks (E_3 and E_4).

As an additional control step, the abundance of Co^{3+} in the individual samples can be estimated by the fit procedure introduced in [12]: Co K-edge experimental reference spectra of two samples with Co^{2+} in ZnO and Co^{3+} in $ZnCo_2O_4$, as also used in Ref. [12], are superimposed to fit the respective measured absorption spectrum. The weighting factor gives the Co^{2+}/Co^{3+} ratio within a few percent accuracy. For the XANES of the sample with the highest Co^{3+} content, the weighing factor that best resembles the measured data is 34.5% Co^{3+} to 65.5% Co^{2+}, the same factor as was determined via the FDMNES simulations. The corresponding 34.5% $ZnCo_2O_4$/65.5% Co:ZnO spectrum is indicated as

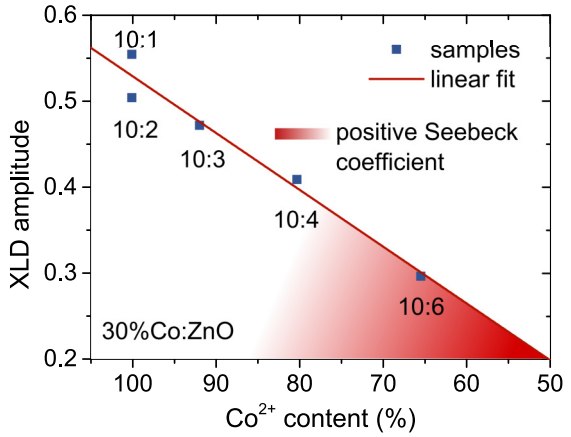

FIG. 4. Co^{2+} content as estimated by a weighted superposition of reference spectra to fit the XANES vs XLD amplitude of the 30% Co:ZnO series. The positive Seebeck coefficient for the sample with the highest Co^{3+} content is qualitatively indicated.

a dotted red line in Fig. 3(c). It resembles the measured experimental spectrum surprisingly well.

Note that, although the crystal structure and local coordination of Co are very different between quasioctahedral Co in wurtzite ZnO and octahedral Co in $ZnCo_2O_4$, the XANES spectra for (simulated) Co in ZnO with two extra oxygen atoms [blue line in Fig. 3(b)] and for (experimental) Co^{3+} in $ZnCo_2O_4$ [blue line in Fig. 3(c)] are very similar. This leads again to the conclusion that the shape and energetic position of the features in the Co absorption spectrum is not very sensitive to the *actual* local geometry of Co and O, but only to the valence state, i.e. the number of bonds of Co.

Figure 4 summarizes the results of the fitting procedure using reference spectra for the entire growth series. As can be seen, the change of the composition ratio, i.e., the shift in valence, correlates linearly with the decrease of the XLD amplitude. This suggests that the amount of Co being present as Co^{3+} is fine-tunable by the provided oxygen partial pressure at the cost of the local crystal structure, but, in contrast to Ref. [12], under retention of the overall wurtzite structure of ZnO. Seebeck measurements show a strongly fluctuating voltage at a low positive value (+0.1 to +2.0 mV), which indicates a positive Seebeck coefficient, i.e., the presence of a *p*-type carrier background, for the specimen with the highest Co^{3+} content. This is qualitatively indicated by the shade in Fig. 4. Obviously, the presence of a certain amount of Co^{3+}, as in *p*-type $ZnCo_2O_4$, provides a sufficiently large *p*-type carrier background to dominate over the intrinsic *n*-type conductivity of (Co-doped) ZnO, although the global crystal remains in its initial wurtzite structure. Therefore, the *p*-type carriers are only generated by the local coordination of Co to O, and they do not require the presence of a spinel structure. This finding is consistent with the fact that also amorphous $ZnCo_2O_4$ is a good *p*-type conductor [9]. Note, however, that the actual carrier concentration could not be determined for our *p*-type Co:ZnO specimen by Hall measurements because of the high resistivity (2.04×10^4 Ω m) and low mobility of the sample.

To increase the hole concentration via an increase of the amount of Co^{3+}, a 50% Co:ZnO concentration series was

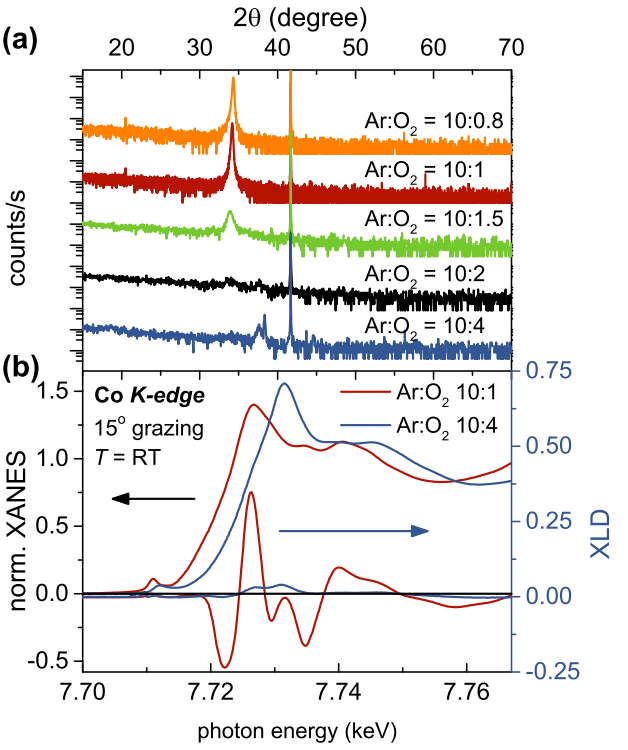

FIG. 5. (a) XRD diffractograms of 50% Co:ZnO grown at varying oxygen partial pressures. (b) Corresponding XANES and XLD spectra for the samples grown with $Ar:O_2$ = 10:1 and 10:4.

fabricated. However, it was not possible to maintain the wurtzite structure and stabilize quasioctahedral, i.e., Co^{3+}, in a similar manner. As can be seen from the XRD diffractograms in Fig. 5(a), the crystalline quality of the ZnO reduces dramatically with increasing $Ar:O_2$ ratio, and the sample is virtually amorphous already at $Ar:O_2$ = 10:2. Obviously, at such high Co concentrations the high oxygen partial pressure leads to a total destabilization of the wurtzite structure. At even higher $Ar:O_2$ ratios, a different crystalline phase with a reflex at 37.6° appears, which we take as a first indication of the onset of the formation of the spinel. Figure 5(b) displays the corresponding XANES and XLD spectra for the samples containing the least (10:1) and the most Co^{3+} (10:4), which corroborates the XRD results. The XANES shifts from a clearly Co^{2+} shape for $Ar:O_2$ = 10:1 to Co^{3+} for the $Ar:O_2$ = 10:4 and also the XLD amplitude almost vanishes for $Ar:O_2$ = 10:4. Interestingly, the absorption spectrum is very similar to that of Co^{3+} in the cubic spinel, see Fig. 3(c), although a pronounced spinel reflex in XRD is still missing. Note, however, that the *p*-type properties of $ZnCo_2O_4$ are maintained even when they are amorphous [9].

A reason for the destabilization of the wurtzite structure at high oxygen partial pressures may be the increased concentrations of Co^{3+}. Since for 30% Co:ZnO only 34.5% of the Co dopants are in the Co^{3+} configuration, the net Co^{3+} cation concentration is 10.4%, which is well below the coalescence limit of 20% for the hcp cationic sublattice [24]. Therefore, no connected paths of such quasioctahedral configurations exist throughout the sample. Obviously, the Co^{3+} concentration is much higher for 50% Co:ZnO. Here

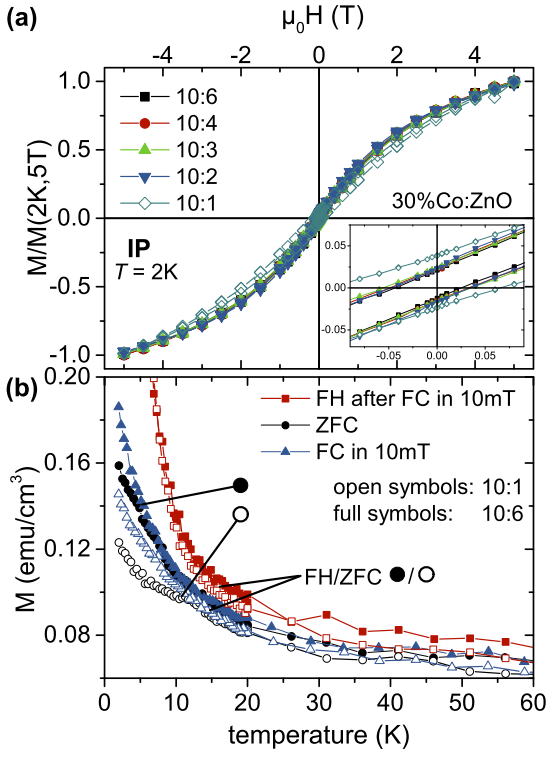

FIG. 6. (a) SQUID IP magnetization curves recorded at 2 K for all samples of the 30% Co:ZnO series. The low-field region is enlarged in the inset. (b) Temperature-dependent magnetization curves for the sample consisting purely of Co^{2+} (10:1, open symbols) and the sample with the highest Co^{3+} content (10:6, full symbol). The respective bifurcation temperatures are indicated.

connected Co^{3+} configurations spread throughout the sample and might lead to the observed destabilization of the wurtzite lattice.

Returning to the stabilization of Co^{3+} in the wurtzite structure for the 30% Co:ZnO specimens, an alternation of the electric properties connotes that also the magnetic properties may be changed (e.g., [3]). Therefore, an in-depth characterization of the magnetic properties has been conducted.

Figure 6(a) displays in-plane SQUID magnetization curves for the entire 30% Co:ZnO series, which were normalized to the maximum magnetization at 2 K and 5 T for better comparability. The magnetization at 2 K and 5 T is 27 emu/cm^3 for 10:1 and 30 emu/cm^3 for 10:6, respectively. All the hystereses are narrowly opened over a wide field range, and they do not saturate up to the maximum attainable field of 5 T. The normalized $M(H)$ curves fall very well atop of each other, but the sample with pure Co^{2+} character exhibits a slightly wider opening of the hysteresis. Additionally, a slight vertical shift of the hystereses is present for all samples, which is also clearly more pronounced for the pure Co^{2+}:ZnO specimen. The occurrence of the hysteretic behavior together with the vertical shift has recently been explained for 60% Co:ZnO by uncompensated antiferromagnetic Co-O-Co-$\cdots$-configurations of different size categories using a Stoner-Wohlfarth-like model [25] and investigated in dependence of the doping concentration in Ref. [26]. The presence of this vertical shift of the hystereses together with a finite slope at 5 T in Fig. 6(a) indicates that 30% Co:ZnO is also an uncompensated antiferromagnet. The decrease of the vertical shift in the samples containing a sizable fraction of Co^{3+}, however, is a noteworthy observation. Obviously, the quasioctahedral coordination, present in all samples besides of the 10:1 specimen, reduces the ability to pin the uncompensated magnetic moments of Co-O-Co...configurations, as introduced in [25]. Figure 6(b) shows the corresponding temperature-dependent magnetization data for the samples with pure Co^{2+} and the highest Co^{3+} fraction recorded at 10 mT applied field. No significant difference between the samples exists, despite a slight deviation of the curves' bifurcation, which can be taken as magnetic order temperature: the bifurcation between FC/ZFC, which shows the contribution of uncompensated moments activated by 10 mT, vanishes already at low temperatures around 5 K (10:6) and 10 K (10:1), respectively. The bifurcation between FH/ZFC, on the other hand, which stands for the uncompensated moments activated by 5 T, i.e., larger configurations, is present up to 15 K, which is consistent with the next-neighbor antiferromagnetic coupling constant at low Co doping [27]. Obviously, the presence of Co^{3+} or hole carriers in the samples does not lead to a more robust magnetization at higher temperatures compared to Co^{2+} in ZnO, but on the contrary it lowers the order temperature for the "smaller" Co-O-Co...configurations, discussed in Refs. [25,26]. This indicates that the magnetic behavior of the samples is still governed by next-neighbor, i.e. short-ranged, coupling mechanisms.

Figure 7(a) shows XANES measurements together with the corresponding element-selective XMCD spectra at the Co K-edge at 2.5 K and 17 T for the two end points (10:1 and 10:6) of the 30% Co:ZnO growth series. Both samples possess a well-defined preedge feature in XMCD at which field-dependent magnetization curves were recorded. The absence of a Co^0 signature in the XMCD as indicated in Fig. 7(a) corroborates the absence of metallic Co as suggested by the size of the XANES preedge feature in Fig. 2(b). Individual features in the XMCD at the main absorption also exist for the magnetic contributions of Co^{2+} and Co^{3+} (see Ref. [12]). They are indicated in Fig. 7(a) and prove that also Co^{3+} contributes to the integral magnetic properties. The XMCD(H) curves have been recorded at the preedge, the Co^{2+} and Co^{3+} energies, and they are shown in Fig. 7(b). Since the signal-to-noise ratio at the preedge is much higher than at the Co^{2+} and Co^{3+} energies, and those two curves fall atop each other within the noise level (see the inset), the following discussion is limited to the measurement at the preedge. Here two observations can be made: (i) up to 17 T the curves are not saturated, which is clear experimental evidence of the antiferromagnetic coupling between the Co cations [27], regardless of whether the samples contain Co^{3+} and are p-type or not; and (ii) the curvature for the pure Co^{2+} sample compared to the highest Co^{3+} content is much weaker. The latter can be explained by an increased magnetic moment of Co^{3+} compared to Co^{2+} in a simplistic spin-only picture. The additional oxygen atoms, and thus the quasioctahedral coordination, leads to an oxidation of the Co atoms from a $3d^7$ to a $3d^6$ state, which presumably changes the resulting spin configuration from $S = 3/2$ for Co^{2+} toward the $S = 2$ state of Co^{3+}, which

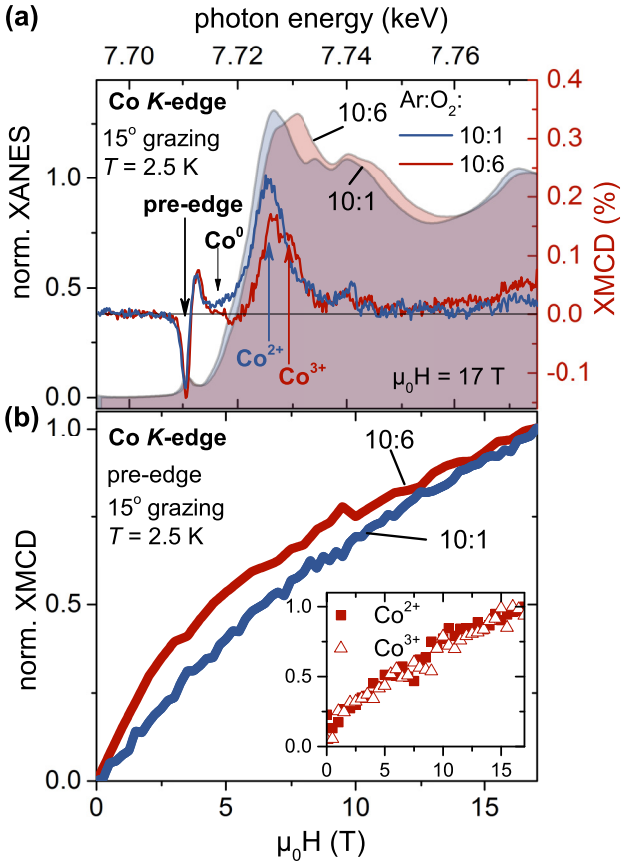

FIG. 7. (a) XANES and XMCD measurements for the 30% Co:ZnO specimens with 10:1 and 10:6 Ar:O_2 ratios during growth. The absorption edge as well as the position of the XMCD main feature shift for higher oxygen ratios. (b) XMCD(H) curves recorded at the preedge energy. The curves are normalized to the maximum magnetization for better comparability. Inset: XMCD(H) curves of the 10:6 sample recorded at the Co^{2+} and Co^{3+} energies. In between the noise level, the two curves overlap.

is energetically close to $S = 0$ state, which is the ground state for a perfect octahedral coordination as in $ZnCo_2O_4$ [28]. This behavior is also observed in the SQUID hystereses and magnetization values in Fig. 6(a) and the XMCD(H) curves in Ref. [12]: the change in carrier concentration and valence of Co only increases the magnetic moment but not the nature of the magnetic coupling. Therefore, the dominant magnetic interaction in Co:ZnO remains uncompensated antiferromagnetism.

IV. CONCLUSION

We discussed the influence of the Co valence on structural and magnetic properties of two series of 30% and 50% Co:ZnO. For high oxygen partial pressures, a Co valence shift from Co^{2+} to Co^{3+} is evidenced in element-selective absorption spectra. The occurrence of Co^{3+} is explained by an interstitial incorporation of additional oxygen atoms and corroborated by FDMNES simulations. Regardless of the valence shift of Co, the crystal retains a wurtzite structure for the 30% series. For 50% Co:ZnO, an increasing Co^{3+} concentration leads to a destabilization of the wurtzite structure, and a spinel phase starts to form. It could be shown that the abundance of Co^{3+} can be linearly increased by the oxygen partial pressure during growth, and that for the highest concentration of Co^{3+} in 30% Co:ZnO a positive Seebeck coefficient indicates a p-type carrier background. The stabilization of Co^{3+} in ZnO, therefore, might be a viable route to enable p-type conductivity in Co:ZnO. While the presence of Co^{3+} and a p-type carrier background does not alter the nature and coupling strength of the uncompensated antiferromagnetism of Co:ZnO, we can report an increased effective magnetic moment per Co dopant atom as well as a reduced vertical exchange biaslike shift. The latter indicates that this effect is caused by the Co^{2+} species only, which will also be of relevance for the A/B disorder of the respective $ZnCo_2O_4$ spinel.

ACKNOWLEDGMENTS

The authors gratefully acknowledge funding by the Austrian Science Fund (FWF)—Project No. P26164-N20. We thank H. von Wenckstern and F. Schein for providing spinel reference samples and the conduction of the Seebeck measurements.

[1] T. Yamamoto and H. Katayama-Yoshida, Jpn. J. Appl. Phys. **38**, L166 (1999).
[2] K. Sato and H. Katayama-Yoshida, Jpn. J. Appl. Phys. **39**, L555 (2000).
[3] T. Dietl, H. Ohno, F. Matsukura, J. Cibert, and D. Ferrand, Science **287**, 1019 (2000).
[4] K. Potzger and S. Zhou, Phys. Status Solidi B **246**, 1147 (2009).
[5] F. Pan, C. Song, X. J. Liu, Y. C. Yang, and F. Zeng, Mater. Sci. Eng. R **62**, 1 (2008).
[6] H. Peng, H. J. Xiang, S.-H. Wei, S.-S. Li, J.-B. Xia, and J. Li, Phys. Rev. Lett. **102**, 017201 (2009).
[7] J. M. D. Coey, M. Venkatesan, and C. B. Fitzgerald, Nat. Mater. **4**, 173 (2005).
[8] Y. Sharma, N. Sharma, G. V. Subba Rao, and B. Chowdari, Adv. Funct. Mater. **17**, 2855 (2007).
[9] F. Schein, H. von Wenckstern, and M. Grundmann, IEEE Electron Dev. Lett. **33**, 676 (2012).
[10] H. J. Kim, I. C. Song, J. H. Sim, H. Kim, Y. E. Ihm, and W. K. Coo, Phys. Status Solidi B **241**, 1553 (2004).
[11] X. Che, L. Li, and G. Li, Appl. Phys. Lett. **108**, 143102 (2016).
[12] B. Henne, V. Ney, K. Ollefs, F. Wilhelm, A. Rogalev, and A. Ney, Sci. Rep. **5**, 16863 (2015).
[13] X.-C. Liu, E.-W. Shi, Z.-Z. Chen, B.-Y. Chen, T. Zhang, L.-X. Song, K.-J. Zhou, M.-Q. Cui, W.-S. Yan, Z. Xie, B. He, and S.-Q. Wei, J. Phys.: Condens. Matter **20**, 025208 (2008).
[14] A. Rogalev, F. Wilhelm, J. Goulon, and G. Goujan, in *Magnetism and Synchrotron Radiation: Towards the Fourth Generation Light Sources*, Springer Proceedings in Physics Vol. 151 (Springer, Berlin, 2013), p. 289.

[15] M. Sawicki, W. Stefanowicz, and A. Ney, Semicond. Sci. Technol. **26**, 064006 (2011).
[16] JCPDS Card No. 89-1397.
[17] E. H. Kisi and M. Elcombe, Acta Cryst. C **45**, 1867 (1989).
[18] A. Ney, A. Kovács, N. Ney, S. Ye, K. Ollefs, T. Kammermeier, F. Wilhelm, A. Rogalev, and R. E. Dunin-Borkowski, New J. Phys. **13**, 103001 (2011).
[19] A. Ney, M. Opel, T. C. Kaspar, V. Ney, S. Ye, K. Ollefs, T. Kammermeier, S. Bauer, K.-W. Nielsen, S. T. B. Goennenwein, M. H. Engelhard, S. Zhou, K. Potzger, J. Simon, W. Mader, S. M. Heald, J. C. Cezar, F. Wilhelm, A. Rogalev, R. Gross, and S. A. Chambers, New J. Phys. **12**, 013020 (2010).
[20] O. Bunau and Y. Joly, J. Phys.: Condens. Matter **21**, 345501 (2009).
[21] A. Ney, V. Ney, K. Ollefs, D. Schauries, F. Wilhelm, and A. Rogalev, J. Surf. Interfac. Mater. **2**, 14 (2014).
[22] A. Ney, Materials **3**, 3565 (2010).
[23] K. Momma and F. Izumi, J. Appl. Cryst. **44**, 1272 (2011).
[24] C. Lorenz, R. May, and R. M. Ziff, J. Stat. Phys. **98**, 961 (2000).
[25] B. Henne, V. Ney, M. de Souza, and A. Ney, Phys. Rev. B **93**, 144406 (2016).
[26] V. Ney, B. Henne, J. Lumetzberger, F. Wilhelm, K. Ollefs, A. Rogalev, A. Kovacs, M. Kieschnick, and A. Ney, Phys. Rev. B **94**, 224405 (2016).
[27] A. Ney, V. Ney, F. Wilhelm, A. Rogalev, and K. Usadel, Phys. Rev. B **85**, 245202 (2012).
[28] P. Cossee, Recueil **75**, 1089 (1956).